

## ROLE OF Au NANOSHEETS IN ENHANCING THE PERFORMANCE OF Yb/ZnS/CdS/Au TUNNELING PHOTODETECTORS

M. ABUSAA<sup>a</sup>, A. F. QASRAWI<sup>a,c,\*</sup>, B. M. ASAAD<sup>a</sup>, H. K. KHANFAR<sup>b</sup>

<sup>a</sup>Department of Physics, Arab American University, Jenin, Palestine

<sup>b</sup>Department of Telecommunication Engineering, Arab American University, Jenin, Palestine

<sup>c</sup>Faculty of Engineering, Atilim University, 06836 Ankara, Turkey

In this study, the effects of Au nanosheets of thicknesses of 50 nm on the structural, electrical and photoelectrical properties of Yb/ZnS/CdS/Au (ZAC-0) devices is considered. Stacked layers of ZnS and CdS which are prepared by the thermal evaporation technique onto Yb substrates under vacuum pressure of  $10^{-5}$  mbar exhibits rectifying characteristics. For these diodes a reverse to forward current ratios of  $\sim 10^5$  at biasing voltage of 0.60 V is determined. Insertion of Au nanosheets between the stacked layers of ZnS and CdS increased the current values by three orders of magnitude and changed the current conduction mechanism from thermionic emission to tunneling under reverse biasing conditions. The ZAC-0 device, exhibit a barrier height lowering and barrier widening upon insertion of Au nanosheets. After the participation of Au nanosheets in the structure of the ZAC-0 devices, large photosensitivity and responsivity accompanied with high external quantum efficiency is observed. The responsivity to 406 nm laser radiation is biasing voltage dependent and reaches 135 mA/W at 0.60 V. The features of the Yb/ZnS/Au/CdS/Au photosensors nominate them as promising candidates for use in light communication technology as signal receivers.

(Received September 6, 2020; Accepted November 10, 2020)

*Keywords:* ZnS/Au/CdS, X-ray, Photodiode, 406 nm laser, External quantum efficiency

### 1. Introduction

Heterojunction devices comprising ZnS/CdS interfaces are of interest owing to their wide range of applications. They find applications as nano and micro-devices. ZnS/CdS heterojunctions are used as photovoltaic quantum dot solar cells [1, 2]. Alloyed  $\text{Cd}_x\text{Zn}_{1-x}\text{S}$  quantum dots which are prepared using the successive ionic layer adsorption and reaction method displayed photoconversion efficiency of 3.6%. The enhanced efficiency is associated with an open-circuit voltage and short circuit current of 0.725 V and  $11.66 \text{ mA cm}^{-2}$  [2]. In addition, stacked layers of ZnS/CdS are observed to exhibit a third order nonlinear optical susceptibility allowing them for applications which are based on nonlinear optical responses [3]. Furthermore, ZnS/CdS structures shows a solar-driven photocatalytic water-splitting features that make them attractive for  $\text{H}_2$  production [4]. As photodiodes, when the ZnS/CdS heterojunctions are participated in the structure of Mo/CZTSe/CdS/ZnS/i-ZnO/ITO photovoltaic devices, they displayed external quantum efficiency values that depends on the spectral energy of incident light. The highest EQE% of value of  $\sim 80\%$  was observed for light of wavelengths of  $\sim 530 \text{ nm}$  [5]. The external quantum efficiency value for blue light ( $\sim 400 \text{ nm}$ ) reaches 55%. The EQE% values for these detectors are strongly affected by the density of interfacial states. The lower the density of interfacial states, the higher the external quantum efficiency and the larger the photocurrent density [5].

Owing to the wide range of applications of ZnS/CdS interfaces and the properties that are associated with its interface density of states, we are motivated to study the structural and electrical properties of the ZnS/CdS interfaces as photodetectors suitable for blue laser light sensing which are used in communication technology. The ZnS/CdS interface states will be disturbed by a 50 nm thick layer of Au in an attempt to enhance its optoelectronic performance.

\* Corresponding author: atef.qasrawi@aaup.edu

Thus, the stacked layers of ZnS/Au/CdS which are coated onto Yb metal and glass substrates will be structurally and photo-electrically characterized to investigate the effects of Au nanosheets on the properties of ZnS/CdS photodiodes.

## 2. Experimental details

ZnS thin films of thicknesses of 500 nm are coated onto ultrasonically cleaned glass and Yb thin film substrates using NORM VCM -600 thermal evaporator. The source material was ZnS crystal lumps (99.99%). The evaporation was actualized with the help of tungsten heaters of boat shapes. Some of the produced glass/ZnS and Yb/ZnS films are coated with Au nanosheets of thickness of 50 nm from high purity gold wires as source materials. The gold layers were then coated with 500 nm thick CdS. The resulting Yb/ZnS/Au/CdS stacked layers is masked and coated with Au pads of areas of  $3.41 \times 10^{-2} \text{ cm}^2$ . The films thicknesses were measured with the help of an Inficon STM-2 thickness monitor attached to the system. The structural characterizations were carried out with the help of  $\text{Cu}_{k\alpha}$  MiniFlex 600 X-ray diffraction unit at scanning speed of 0.50 deg./min. The current- voltage characteristics curves were recorded with the help of programmable Keithley I-V system. Light irradiation was supplied from THORLAB diode laser of wavelengths of 406 nm and power of 5.5 mW.

## 3. Results and discussion

In this article, we focus on improving the structural, electrical and photoelectrical properties of the ZnS/CdS interfaces through insertion of metal nanosheets as conducting layer between the ZnS and CdS thin layers. The schematics of the device under study are illustrated in inset-1 of Fig. 1. The heterojunction devices not comprising Au nanosheets are called ZAC-0 nm. Those which have Au slabs of thicknesses of 50 nm are called ZAC-50. The X-ray diffraction patterns for ZAC-0 and ZAC-50 heterojunctions are shown in Fig. 1. The analyses of the observed sharp X-ray diffraction patterns were carried out with the help of "TREOR 92" software packages and were also compared with the existing literature data [6]. Two of the observed three diffraction peak are centered at diffraction angles of  $2\theta = 24.75^\circ$  and at  $2\theta = 27.45^\circ$  are assigned to the hexagonal CdS with lattice parameters of  $a = b = 4.152 \text{ \AA}$  and  $c = 6.493 \text{ \AA}$ . The third peak which is observed at  $2\theta = 29.30^\circ$  is assigned to the cubic ZnS. The lattice parameters for the ZnS are  $a = b = c = 5.274 \text{ \AA}$ . The values of the lattice parameters of the ZnS coated onto Yb substrates are close to the previously reported as  $5.333 \text{ \AA}$ . As can be seen from inset-2 of Fig. 1, the maximum peak of CdS along the (002) direction is shifted toward smaller angles. The structural calculations have shown that insertion of Au nanosheets between ZnS and CdS layers shifted the values of the lattice constants of CdS from  $a = b = 4.152 \text{ \AA}$  to  $a = b = 4.193 \text{ \AA}$  and from  $c = 6.493 \text{ \AA}$  to  $c = 6.575 \text{ \AA}$ , respectively. An extension in the lattice constants values of CdS by 1.0% and by 1.26% is observed upon Au nanosheets participation. The lattice constant of ZnS is not affected by the Au nanosheets.

On the other hand, the calculated mechanical parameters including crystallite size ( $D$ ), microstrain ( $\epsilon$ ), defect density ( $\delta$ ) and stacking faults (SF%) using the previously reported [6] equations revealed respective values of 29 nm,  $5.19 \times 10^{-3}$ ,  $2.44 \times 10^{11} \text{ lines/cm}^2$  and 0.259%. These parameters exhibit values of 28 nm,  $5.43 \times 10^{-3}$ ,  $5.07 \times 10^{11} \text{ lines/cm}^2$  and 0.352%, respectively, upon insertion of Au nanosheets between ZnS and CdS interfacing layers. Remarkable increase in the defect density and in the stacking fault percentages is observed. One of the reasons that could account for the increased defect density is the lattice mismatches that are formed between Au nanosheets and CdS films. The lattice mismatches ( $\Delta\% = |a^{\text{CdS}} - a^{\text{Au}}|/a^{\text{CdS}}$ ;  $a^{\text{Au}} = 4.08 \text{ \AA}$ ) are 1.73% along the  $a$ -axis and 37.1% along the  $c$ -axis. The lattice mismatches between ZnS and CdS in the absence of Au nanosheets is  $\Delta\% = |a^{\text{CdS}} - a^{\text{ZnS}}|/a^{\text{CdS}} = 27.0\%$  along the  $a$ -axis and 23.11% along the  $c$ -axis. The numerical data suggest that the

lattice mismatches along the  $a$  –axis remarkable decreased and increased along the  $c$  –axis as a result of insertion of Au nanosheets between stacked layers of ZnS and CdS. Earlier reports which considered heterojunction structures mentioned that, that the larger the lattice mismatches between stacked layers, the larger the applied strain required to modulate the electronic properties [8]. It is also reported that large lattice mismatches cause the high lattice strain, defects and misfit strain in the films that in turn lead to the formation of a better polycrystalline structure [9]. These lattice mismatches induced effects are usually accompanied with large defect densities [10] as we also observed here.

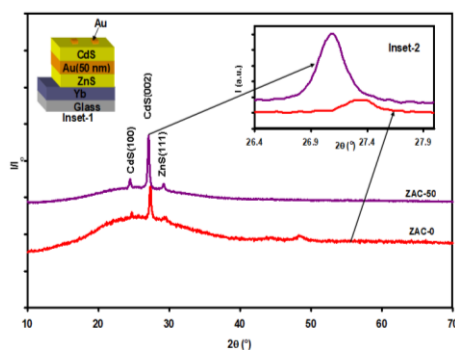


Fig. 1 the X-ray diffraction patterns for the ZnS/CdS heterojunctions before and after the insertion of Au nanosheets. Inset-1 show the schematics of the device and inset-2 shows the maximum peak shift as a result of Au nanosheet insertion.

From electrical point of view, the electron affinities ( $q\chi$ ) of ZnS and CdS are 3.8 eV [11] and 4.5 eV [12], respectively. The respective energy band gap ( $E_g$ ) values are 3.40 eV [6] and 2.41 eV [7]. In accordance with these data the conduction ( $\Delta E_c = |q\chi_{CdS} - q\chi_{ZnS}|$ ) and valence band ( $\Delta E_v = |\Delta E_g - \Delta E_c|$ ) offsets between ZnS and CdS are 0.70 and 0.29 eV, respectively. The band offsets are large enough to cause quantum confinement that is necessary for optoelectronic applications. The quantum confinement leads to energy sub-bands in both conduction and valence bands [13]. Earlier studies on CdSe/ZnS have shown that the quantum confinement can result in the changes of the density of states for both electrons and phonons and as a result it alters the mechanisms of electron-hole recombination [14] mechanisms. Remembering that the electronic configuration of Au ( $4f^{14} 5d^{10} 6s^1$ ) which is at higher orbital energy levels than Zn ( $3d^{10} 4s^2$ ), Cd ( $4d^{10} 5s^2$ ) and S ( $3s^2 3p^4$ ), then, the presence of Au nanosheets forces more atomic orbital overlapping in both of the ZnS and CdS leading to an enrichment of the energy sub-bands. In heterojunctions comprising organic/inorganic systems, the presence of metal nanosheets between layers of ZnS is reported to enhance the quantum confinement effect leading to a blue shift in the band gap [15]. Thus the incorporation of Au nanosheets in between stacked layers of ZnS and CdS is supposed to improve the photoresponsivity ( $R$ ), photocurrent ( $I_{ph}$ ) values and external quantum efficiency ( $EQE\%$ ) of the heterojunction devices which are very sensitive to the quantum confinement effect.

To confirm that the 50 nm thick Au nanosheets have improved the optoelectronic properties of the ZnS/CdS photodiodes, the dark ( $I_d$ ) and illuminated ( $I_l$ ) current ( $I$ )-voltage ( $V$ ) characteristics were recorded. The light irradiation were supplied with the help of diode lasers of wavelengths of 406 nm. The dark  $I-V$  characteristics for the Yb/ZnS/CdS/Au and Yb/ZnS/Au/CdS/Au devices are illustrated in Fig. 2 (a). It is clear from the figure that the presence of Au nanosheets between layers of ZnS and CdS highly increased the dark current values. While the ZAC-0 device display higher  $I_R$  values under reverse biasing conditions compared to the forward one, the ZAC-50 devices displayed higher currents value ( $I_F$ ) under forward biasing conditions. In addition, at particular forward biasing voltage, the current values in ZAC-50 devices are, approximately, five orders of magnitude higher than that of ZAC-0 devices. Moreover, under

reverse biasing conditions, the reverse current values in ZAC-50 devices is three orders of magnitude larger than that of ZAC-0 devices. It is also noticeable that for the ZAC-50 devices, under forward biasing conditions,  $I_F$  exhibit a jump from low current to high current values at biasing voltage of 0.09 V which is very close to the least required thermal energy value ( $3kT=0.08$  V) for electrons to leave the surface of the valence band. As  $V > 3kT$ ,  $I_F$  increases by 22 times.

Analysis which targeted investigation of the current conduction mechanism in the photodiodes was deeply considered. The validity of Schottky-Richardson thermionic emission of charge carriers over energy barriers of heights  $\phi_b$  and/or electric field assisted thermionic emission (tunneling) of charge carriers through electric field dependent potential barriers ( $\Phi$ ) were tested using the respective equations [6, 15, 16],

$$I = AA^*T^2 e^{-\frac{q\phi_b}{kT}} \left( e^{\frac{qV}{nkT}} - 1 \right) \quad (1)$$

and

$$I = AA^{**}T^2 V^\gamma \exp\left(-\frac{e\Phi}{kT}\right) \quad (2)$$

with

$$\Phi = \phi_0 - n\sqrt{\frac{e\eta}{4\pi\epsilon_0\epsilon_r}} \sqrt{V}/\sqrt{w} . \quad (3)$$

In these equations,  $\phi_0$  is the zero field value,  $A^{**}=120m^*$  is the Richardson constant,  $m_{h-ZnS}^* = 0.23 m_o$  [17],  $m_{h-CdS}^* = 0.64m_o$  [17] and  $m_{ZAC-0}^* = (m_{h-ZnS}^{*-1} + m_{h-CdS}^{*-1})^{-1} = 0.169m_o$  for ZnS, CdS and for ZnS/CdS, respectively. The effective mass for electrons in ZAC-50 devices is  $m_{ZAC-50}^* = (m_{h-ZnS}^{*-1} + m_{h-CdS}^{*-1} + m_{e-Au}^{*-1})^{-1} = 0.147m_o$ . Here,  $m_{e-Au}^* = 1.14m_o$  [18] and  $w$  is the net effective width of the interface depletion region. The dielectric constant ( $\epsilon_r$ ) values were taken as 4.8 for Yb/ZnS and 4.5 for CdS. The effective dielectric constant was calculated from the relation,  $\epsilon_r^{eff} = (\epsilon_{r-Yb/ZnS}^{-1} + \epsilon_{r-CdS}^{-1})^{-1} = 2.23$ . Under the conditions where the Schottky-Richardson field emission mechanism dominates, the ideality factor  $n = \eta = 1$ ,  $\gamma = 0$  are substituted. For the ZAC-0 device, Fig. 2 (b) shows  $\ln(I) - V$  and  $\ln(I) - \sqrt{V}$  variations which are linear with acceptable  $R^2$  (measure of deviation of data points from the mean) values under reverse and forward biasing conditions, respectively. The slopes and intercepts of the linear plots which are shown by solid lines, in the figure allow determining the potential barrier height  $\phi_b = 0.88$  eV and ideality factor ( $n$ ) of 3.4 for the reverse biased device and a zero field barrier height ( $\phi_0$ ) of 1.15 eV and barrier width of 2.3 nm for the forward biased device. The data suggests that the current conduction mechanism in the ZAC-0 device is dominated by tunneling of electrons through a high barrier (1.15 eV) of width of 2.4 nm when forward biased (CdS side) and by thermionic emission of charge carriers over a lower potential barrier (0.88 eV) when reverse biased.

The linear plots of the  $\ln(I) - \sqrt{V}$  variations which are presented in Fig. 5 (d) assure the validity of the field assisted thermionic emission or tunneling current transport through ZAC-50 devices. The slopes and intercepts of the  $\ln(I) - \sqrt{V}$  variations which are shown by solid lines in Fig. 5 (d) allowed determining the values of  $\phi_0$  and  $w$  as 0.60 eV and 41.4 nm and 0.68 eV and 39.81 nm, under forward and reverse biasing conditions, respectively.

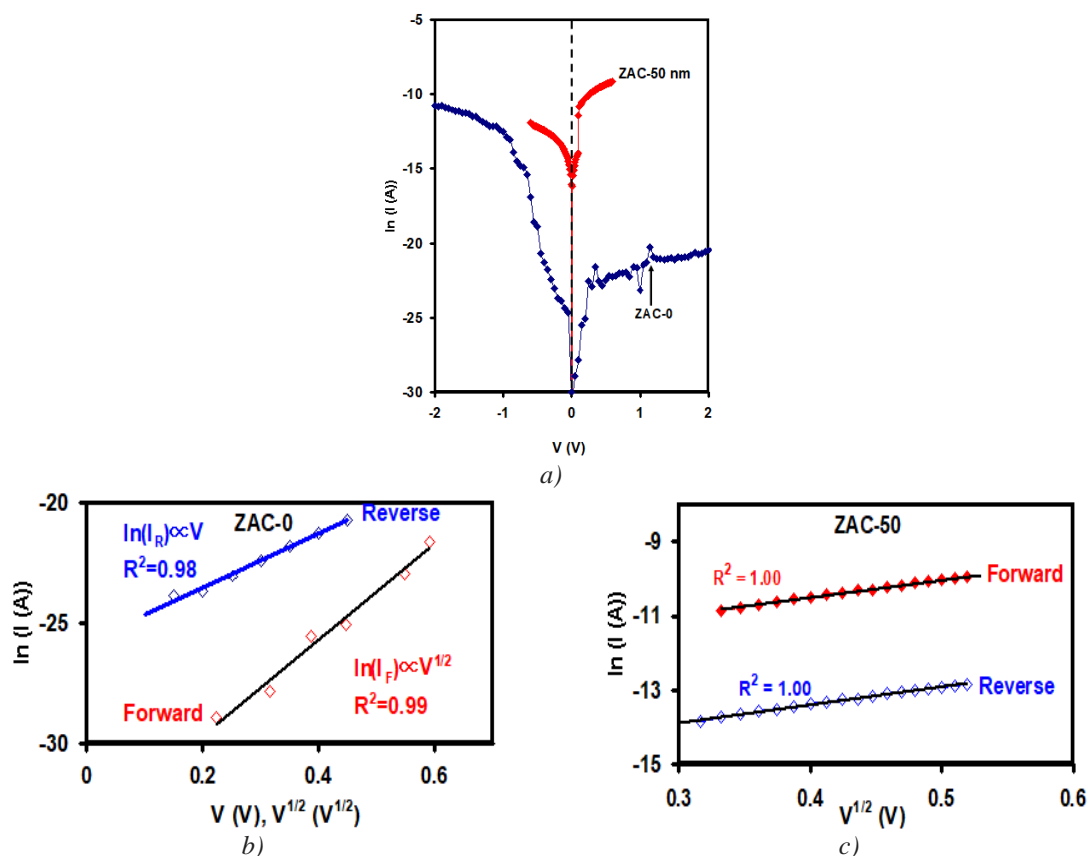


Fig. 2. (a) The  $\ln(I) - V$  characteristics for the Yb/ZnS/CdS/Au devices before and after the insertion of Au nanosheets, (b)  $\ln(I) - V$  and  $\ln(I) - \sqrt{V}$  dependence for the Yb/ZnS/CdS/Au devices before the insertion of Au nanosheets and (c)  $\ln(I) - \sqrt{V}$  dependence for the Yb/ZnS/Au/CdS/Au devices after the insertion of Au nanosheets.

As expected, the orbital overlapping of the Au highly decreased the barrier height from  $\sim 1.15$  eV to 0.60 eV. It also widens the tunneling barrier significantly. The barrier height decreases due to a smaller separation of electron sub-bands and hole sub-bands [19] by orbital overlapping. It is also possible to think that Au nanosheets could behave as doping agents leading to heavy doping effect in which the tunneling current conduction mechanism becomes preferable. Since the ionic radius of  $\text{Au}^{+3}$  in square-planar coordination is 68 pm [20] is smaller than that of  $\text{Zn}^{+2}$  (74 pm [21]) or that of  $\text{Cd}^{+2}$  (96 pm [7]), Au ions can easily occupy vacant sites of Zn or Cd. In addition,  $\text{Au}^{+1}$  with the ionic radius 137 pm [22], can reserve interstitial sites and behave as doping agents. In such processes which include heavy doping effect, the image force lowering effect dominates. It is well known that at higher doping levels the barrier height decreases because of stronger image forces lowering [16].

Attempts to record stable  $I - V$  characteristics for the ZAC-0 devices under 406 nm laser irradiations of power of 5.5 mW were unsuccessful. However, when the ZAC-50 devices were subject to the same irradiation conditions, large photoresponse is observed. Fig. 3 (a) show the dark and illuminated current ( $I_L$ )-voltage characteristic curves for the ZAC-50 devices. It is clear from the figure that the values of  $I_R$  highly increased upon laser irradiation indicating that the generation of electron-hole pairs in the sample become more effective and pronounced as a result of insertion of Au nanosheets between layers of ZnS and CdS. No remarkable effect is observed in the forward current values until the applied forward voltage exceeds 0.51 V. Above this critical voltage, illuminated current exhibits higher values than those dark ones. It may have resulted from the high electric field injection effects. As the forward current is dominated by recombination of charge carriers and reverse current is by generation, it is possible to conclude that the Au

nanosheets have no effect on the recombination dynamics under low injection conditions [16]. Calculations which targeted estimation of the barrier height and barrier width under lasers irradiation ended with the result that the ZAC-50 devices exhibit a zero field barrier height of  $\phi_0 = 0.53$  eV and barrier width ( $w$ ) of 24.22 nm under reverse biasing conditions. The values of  $\phi_0$  and  $w$  under forward biasing conditions are also determined and found to be 0.56 eV and 31.06 nm, respectively. It is clear that the barrier height lowers and the barrier width narrows under light irradiations owing to enhanced quantum confinements in CdS which resulted from Au nanosheets. The original investigations of quantum confinement effect indicated that the long time illumination decreases the barrier height resulting in more effective holes captures and larger relaxation rate [23]. In addition, the barrier lowering upon light excitations can also be assigned to Fermi level shift towards the intrinsic Fermi level [24]. It is reported that barriers are produced due to the existence of surface states in the photosites. The photo-excited surface states may induce surface band-bending that in turn creates accumulation or depletion layers with a static space-charge region at the interface. Such barrier formation causes an energy difference between impurity levels and the acceptor/donor and valence/conduction bands, leading to significant change in the light absorption properties [25].

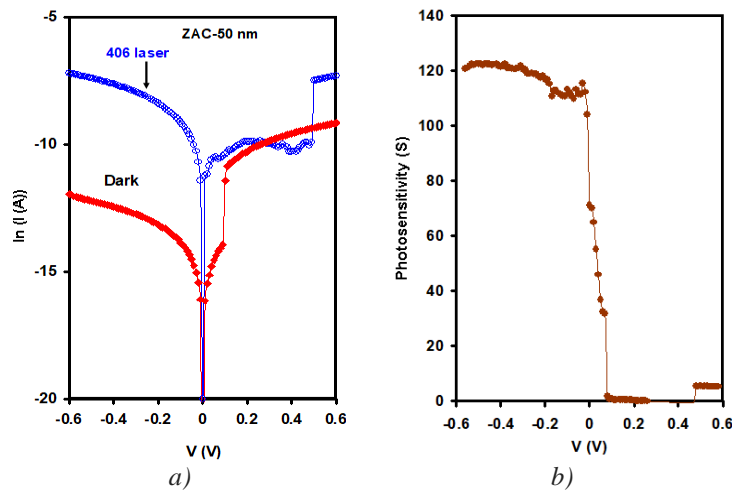


Fig. 3. (a) the  $\ln(I) - V$  characteristics in the dark and under laser light irradiation and (b) the biasing voltage dependent photosensitivity for Yb/ZnS/Au/CdS/Au devices.

Fig. 3 (b) display the ZAC-50 device photosensitivity ( $S = \frac{I_{ph}}{I_d}$ ;  $I_{ph}$  is photocurrent) as function of biasing voltage. High photosensitivity is observed for the samples under reverse biasing conditions. While the ZAC-50 devices display no remarkable photosensitivity under forward biasing conditions in the range of (0.12-0.60 V), the photosensitivity slowly increases with increasing reverse voltage in the low field injection range (0.10-0.40 V) for larger applied reverse voltages,  $S$  tends to remain constant exhibiting an average value of 121. Sharp transition from low  $S$  to high  $S$  values is observed as the device work in the voltage range from +0.12 to -0.10 V. The large photosensitivity to laser light sensing makes the ZAC-50 devices attractive for use in light communications as signal receivers. For these issues, the knowledge of the photodiode parameters is of interest. For this reason, the diode responsivity ( $\tilde{R} = I_{ph}/p_{opt}$ ;  $p_{opt}$  is the optical power of radiation source) and the external quantum efficiency ( $EQE\% = 100 \cdot \frac{\tilde{R} \cdot h\nu}{q}$ ;  $h\nu$  is incident light energy) are calculated for the reverse biased device and presented in Fig. 4 (a) and (b), respectively. As seen from the figure, linearly increasing  $\tilde{R}$  and  $EQE\%$  with increasing reverse bias voltage is observed. The responsivity of the ZAC-50 light receivers reaches 135 mA/W at 0.60 V. The high responsivity is associated with acceptable values of external quantum efficiency. The external quantum efficiency percentage reaches 41.3% at 0.60 V. The deviation of the external quantum efficiency from 100% could be assigned to

current loss by recombination, incompleteness of absorption and reflection [16]. Compared to recent works [5] for the ZnS/CdS interfaces to reach ~55% at 400 nm, they should be inserted into a complex structure of stacked layers like Mo/CZTSe/CdS/ZnS/i-ZnO/ITO [5]. The work here shows that by the insertion of 50 nm thick Au nanosheets, it is possible to achieve comparable values of external quantum efficiency without participation in a complicated structure.

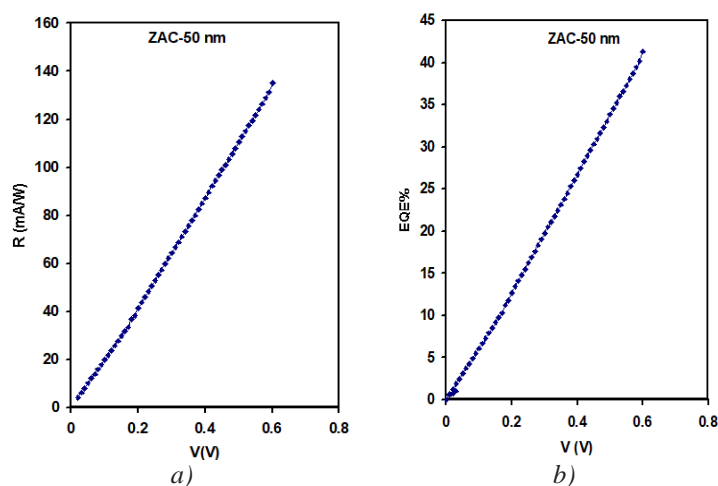


Fig. 4. (a) the responsivity and (b) the external quantum efficiency as function of reverse biased voltage for Yb/ZnS/Au/CdS/Au devices.

#### 4. Conclusions

In the current study, we have shown that the structural parameters, the electrical and photodetection properties of stacked layers of ZnS and CdS could be enhanced via Au nanosandwiching. Insertion of 50 nm thick layers of Au was sufficient to abruptly alter the physical nature and current conduction mechanisms in the heterojunction devices. A barrier height lowering and depletion width widening in the nanoscale level is achieved via Au nanosheets. The ZnS/Au/CdS stacked layers which are coated onto Yb thin film substrates displayed good photodetector characteristics in response to blue light lasers. The external quantum efficiency and light responsivity are sufficiently large nominating the Yb/ZnS/Au/CdS/Au devices for optoelectronic applications.

#### Acknowledgments

This work was carried out at the Arab American University-Palestine (AAUP) laboratories with the support of the scientific research council (SRC). For this reason, the authors acknowledge with thanks the SRC of AAUP for the financial and technical support.

#### References

- [1] Zhen Li, Libo Yu, *Materials* **12**(10), 1583 (2019).
- [2] Omar E. Solis, Jesus Manuel Rivas, Tzarara Lopez-Luke, Isaac Zarazua, Jorge de la Torre, Diego Esparza, *IEEE Journal of Photovoltaics* (2020).
- [3] N. Zeiri, A. Naifar, S. Abdi-Ben Nasrallah, M. Said, *Physica Scripta* **95**(1), 017001 (2019).
- [4] Bowen Sun, Hui Wang, Jiakun Wu, Yanling Geng, Jixiang Xu, Yaowei Wang, Yanyan Li, Haifeng Lin, Lei Wang, *Cryst. Eng. Comm.* **22**(16), 2743 (2020).
- [5] Viviana Hernández-Calderón, Osvaldo Vigil-Galán, Maxim Guc, Alexis Carrillo-Osuna,

- Sergio Ramirez Velasco, Fernando J. Sánchez-Rodríguez, Pedro Vidal-Fuentes, Sergio Giraldo, Edgardo Saucedo, Yudania Sánchez, ACS Applied Energy Materials (2020).
- [6] Najla M. Khusayfan, S. E. Al Garni, A. F. Qasrawi, Current Applied Physics **17**(1), 115 (2017).
- [7] Tamara Y. Abed, A. F. Qasrawi, S. E. Al Garni, Journal of Alloys and Compounds **731**, 1022 (2018).
- [8] Dongchao Wang, Li Chen, Xiaoli Wang, Guangliang Cui, Pinhua Zhang, Physical Chemistry Chemical Physics **17**(40), 26979 (2015).
- [9] Seung Wook Shin, G. L. Agawane, In Young Kim, Ye Bin Kwon, In Ok Jung, Myeng Gil Gang, A. V. Moholkar, Jong-Ha Moon, Jin Hyeok Kim, Jeong Yong Lee, Applied surface science **258**(12), 5073 (2012).
- [10] Xiaolan Zhou, Ilan Stern, Punam Silwal, Ludi Miao, Dae Ho Kim, Applied Physics Letters **100**(3), 032902 (2012).
- [11] Motmaen Aytak, Ali Rostami, Matloub Samiye, Scientific Reports (Nature Publisher Group) **10**(1), (2020).
- [12] Zhijun Ning, Matyas Molnár, Yun Chen, Peter Friberg, Liming Gan, Hans Ågren, Ying Fu, Physical Chemistry Chemical Physics **13**(13), 5848 (2011).
- [13] Greg Sun, R. A. Soref, H. H. Cheng, Optics express **18**(19), 19957 (2010).
- [14] W. Z. Lee, G. W. Shu, J. S. Wang, J. L. Shen, C. A. Lin, W. H. Chang, R. C. Ruaan, Wu-Ching Chou, C. H. Lu, Y. C. Lee, Nanotechnology **16**(9), 1517 (2005).
- [15] A. F. Qasrawi, Hazem K. Khanfar, IEEE Sensors Journal (2020).
- [16] Simon M. Sze, Kwok K. Ng, Physics of semiconductor devices. John wiley & sons, 2006.
- [17] Otfried Madelung, Semiconductors: data handbook, Springer Science & Business Media, 2012.
- [18] Mutsumi Suzuki, Toshiaki Kusunoki, Hiroyuki Shinada, Tomio Yaguchi, Journal of Vacuum Science & Technology B: Microelectronics and Nanometer Structures Processing, Measurement, and Phenomena **13**(6), 2201 (1995).
- [19] W. L. Li, Y. K. Su, D. H. Jaw, IEEE journal of quantum electronics **33**(3), 416 (1997).
- [20] E. M. Kopnin, S. M. Loureiro, T. Asaka, Y. Anan, Y. Matsui, E. Takayama-Muromachi, Chemistry of materials **13**(9), 2905 (2001).
- [21] Aiqin Mao, Hou-Zheng Xiang, Zhan-Guo Zhang, Koji Kuramoto, Hui Zhang, Yanggang Jia, Journal of Magnetism and Magnetic Materials **497**, 165884 (2020).
- [22] R. Terzioglu, G. Aydin, N. Soylu Koc, C. Terzioglu, Journal of Materials Science: Materials in Electronics **30**(3), 2265 (2019).
- [23] N. P. Stepina, A. I. Yakimov, A. V. Nenashev, A. V. Dvurechenskii, A. V. Peregoedov, A. I. Nikiforov, Physica Status Solidi (C) **2**(8), 3118 (2005).
- [24] J. De Wild, E. V. Robert, B. El Adib, D. Abou-Ras, P. J. Dale, Sol. Energ. Mat. Sol. C **157**, 259 (2016).
- [25] L. Shi, S. W. Feng, C. S. Guo, H. Zhu, Degradation and recovery property of Schottky Barrier height of AlGaIn/GaN high electron mobility transistors under reverse AC electrical stress, In 2012 IEEE 11th International Conference on Solid-State and Integrated Circuit Technology (pp. 1-3).